iScience

CellPress
OPEN ACCESS

Article

Gold(III)-P-chirogenic complex induces mitochondrial dysfunction in triple-negative breast cancer

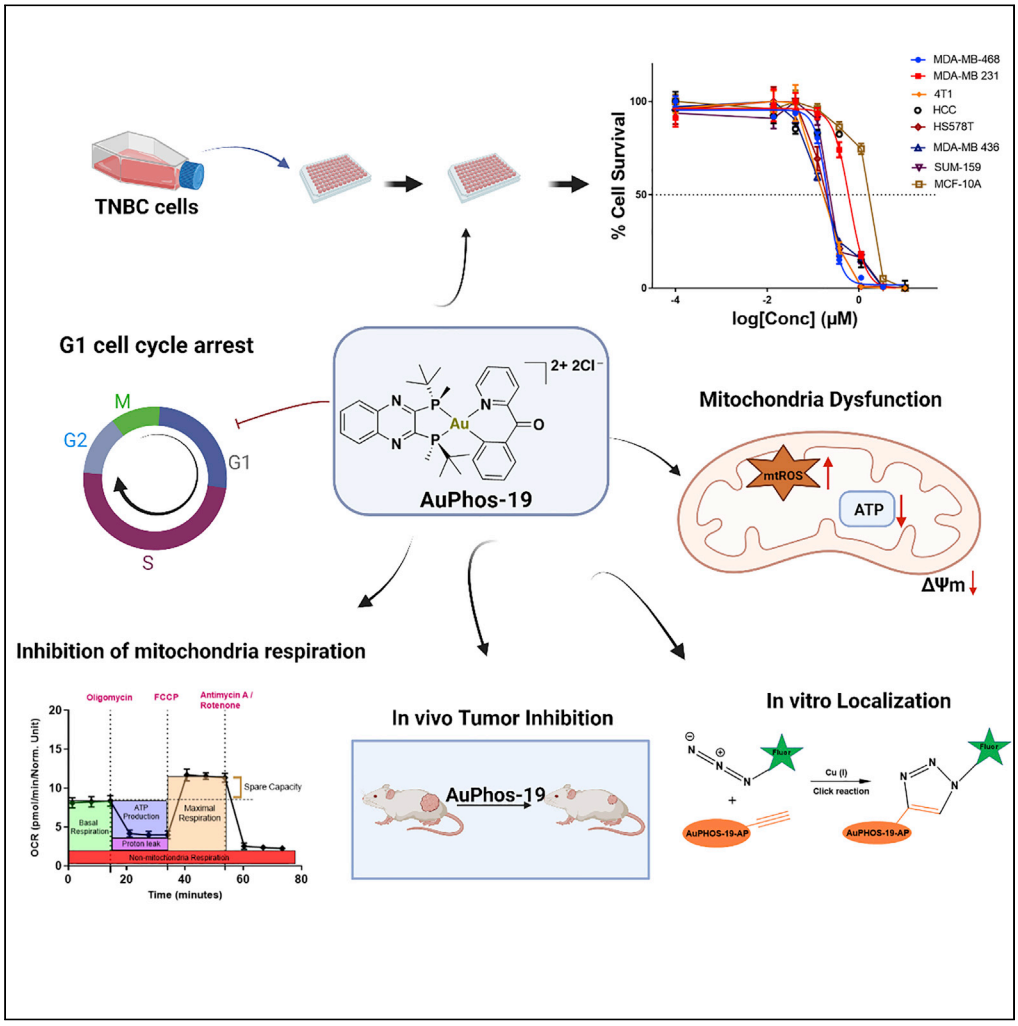

Chibuzor Olelewe, Jong Hyun Kim, Samuel Ofori, Randall T. Mertens, Sailajah Gukathasan, Samuel G. Awuah

awuah@uky.edu

Highlights

AuPhos-19 is effective against different TNBC subtypes

AuPhos-19 inhibits metabolism in TNBC cells to induce AMPK activation

Localization studies reveal that AuPhos-19 accumulates in the mitochondria of TNBC

AuPhos-19 demonstrates modest efficacy *in vivo*

Olelewe et al., iScience *25*, 104340
May 20, 2022 © 2022
https://doi.org/10.1016/j.isci.2022.104340

iScience

CellPress
OPEN ACCESS

Article

Gold(III)-P-chirogenic complex induces mitochondrial dysfunction in triple-negative breast cancer

Chibuzor Olelewe,[1] Jong Hyun Kim,[1] Samuel Ofori,[1] Randall T. Mertens,[1] Sailajah Gukathasan,[1] and Samuel G. Awuah[1,2,3,4,*]

SUMMARY

Chemical agents that specifically exploit metabolic vulnerabilities of cancer cells will be beneficial but are rare. The role of oxidative phosphorylation (OXPHOS) in promoting and maintaining triple-negative breast cancer (TNBC) growth provides new treatment opportunity. In this work, we describe AuPhos-19, a small-molecule gold(III)-based agent bearing a chiral phosphine ligand that selectively disrupts mitochondrial metabolism in murine and human TNBC cells but not normal epithelial cells. AuPhos-19 induces potent cytotoxic effect with half maximal inhibitory concentration (IC_{50}) in the nanomolar range (220–650 nM) across different TNBC cell lines. The lipophilic cationic character of AuPhos-19 facilitates interaction with mitochondrial OXPHOS. AuPhos-19 inhibits mitochondria respiration and induces significant AMPK activation. Depolarization of the mitochondria membrane, mitochondria ROS accumulation, and mitochondria DNA depletion provided further indication that AuPhos-19 perturbs mitochondria function. AuPhos-19 inhibits tumor growth in tumor-bearing mice. This study highlights the development of gold-based compounds targeting mitochondrial pathways for efficacious cancer treatment.

INTRODUCTION

Triple-negative breast cancer (TNBC) is well characterized by the lack of expression of estrogen (ER), progesterone (PR), and the human epidermal growth factor receptor 2 (HER2) receptors. It accounts for nearly 15% of breast cancer cases and has the worst prognosis of all breast cancer subtypes (Dawson et al., 2009; Lin et al., 2012). Significant research effort to improve patient response to therapy via targeting tumors that express ER, PR, and HER2 receptors has yielded transformative outcomes. However, novel therapies for patients diagnosed with TNBC remain a clinical challenge. Thus, the identification and development of new drugs effective against TNBC cells remain an unmet need (Hudis and Gianni, 2011). Given that the conventional cell-surface receptors that allow for therapeutic targeting in other breast cancers are absent in TNBCs, interfering with their metabolic process may represent an effective paradigm to eliminate these cancer cells (Pelicano et al., 2014).

Metabolism is important for energy production and formation of building blocks needed to drive tumorigenesis. This is due to the higher energy demand needed for survival of malignant cells compared with the normal cells. A phenomenon referred to as the Warburg effect came into prominence in the 1920s when Otto Warburg described his observation that cancer cells have high utilization of glucose and high lactate secretion even in the presence of oxygen (Warburg, 1956). This suggested that glycolysis is enhanced in cancer cells unlike normal cells that generate energy via aerobic metabolism (pyruvate oxidation in the mitochondria) (Warburg, 1956). Warburg's observation led to the assumption that mitochondria metabolism is impaired in cancer cells; however, technological advancements over the past couple of decades have aided greater investigation into the role of mitochondria function. Increasing evidence suggest that mitochondria are functional in cancer cells to produce energy (ATP) via oxidative phosphorylation (OXPHOS) needed to support tumorigenesis (Ashton et al., 2018; Kim and DeBerardinis, 2019; Weinberg and Chandel, 2015).

The process of oxidative phosphorylation involves the transfer of electrons from electron donors (e.g. NADH, $FADH_2$, and succinate) to molecular oxygen (O_2) by a series of transmembrane proteins (electron

[1]Department of Chemistry, University of Kentucky, Lexington, KY 40506, USA

[2]Center for Pharmaceutical Research and Innovation, College of Pharmacy and Department of Pharmaceutical Sciences, College of Pharmacy, University of Kentucky, Lexington, KY 40536, USA

[3]Markey Cancer Center, University of Kentucky, Lexington, KY 40536, USA

[4]Lead contact

*Correspondence: awuah@uky.edu

https://doi.org/10.1016/j.isci.2022.104340

carriers) which make up the electron transport chain (ETC) (Ashton et al., 2018). This transfer of electrons through the ETC is used to drive the synthesis of ATP when an electrochemical proton gradient is established across the mitochondrial inner membrane with the aid of ATP synthase (Ashton et al., 2018). Several studies have shown that OXPHOS dependence is high in several cancer types including the recalcitrant TNBC and drives metastasis. Therefore, inhibiting OXPHOS to disrupt the metabolic process in these tumors may represent an effective treatment approach (Masoud et al., 2020; Raninga et al., 2020; Sancho et al., 2016; Shi et al., 2019; Urra et al., 2018).

Platinum-based drugs are still widely used as the standard of care in the treatment of various forms of human malignancies including testicular, cervical, lung, bladder, ovarian, prostate, and breast cancers. However, patients suffer relapse after treatment due to innate resistance or resistance acquired over cycles of chemotherapy (Cimino et al., 2013; Kelland, 2007). In order to improve treatment options and survival outcome of patients with cancer, different classes of metal complexes have been thoroughly investigated and developed including palladium, ruthenium, silver, and gold complexes (Ndagi et al., 2017). Among these classes of compounds, gold-based complexes have gathered attention in recent years due to the anticancer effect that has been shown to be different from cisplatin mode of action. The use of clinically approved gold salts such as auranofin and myochrysine for the treatment of rheumatoid arthritis (Rindfleisch and Muller, 2005) provides great impetus for gold anticancer drug discovery. Several gold complexes existing in Au (I) and (III) oxidation states have been reported to target thiol-containing enzymes (glutathione and thioredoxin reductase) (Rigobello et al., 2004; Zou et al., 2015), proteasome deubiquitinases (Milacic and Dou, 2009; Zou et al., 2016), and the mitochondria (Barnard and Berners-Price, 2007; Rackham et al., 2007). Interestingly, some of these gold complexes have been reported to be potent against the clinically challenging TNBC both *in vitro* and *in vivo* (Arojojoye et al., 2020; Kim et al., 2021; Mertens et al., 2020; Nardon et al., 2014; Ortega et al., 2020; Yeo et al., 2018). These developments highlight the potential that exist in developing gold-based compounds for chemotherapeutic application.

Herein, we report the identification of AuPhos-19, a cyclometalated gold(III) complex, as a cancer-specific inhibitor that interferes with metabolic demands of TNBC. This complex inhibits TNBC proliferation with half maximal inhibitory concentration (IC_{50}) within the nanomolar range (220–650 nM) across different TNBC cell lines (MDA-MB-468, MDA-MB-231, 4T1, and HCC1937). The mammary epithelial cell line MCF10A was used as the normal cell line. We carried out functional assays to gain insight into the mechanism of action of AuPhos-19 which implicated OXPHOS as a potential target. AuPhos-19 inhibited mitochondria respiration to induce significant AMPK activation. This compound significantly depolarized the mitochondria membrane in TNBC cells and caused accumulation of mitochondria ROS. In addition, AuPhos-19 inhibits mitochondria DNA synthesis which might be because of mtROS production. Further indication that AuPhos-19 perturbs mitochondria function was observed in the form of ATF4 induction in response to mitochondria stress. We evaluated the efficacy of AuPhos-19 in metastatic 4T1-iRFP TNBC xenograft mouse model and found moderate inhibition of tumor growth. Our study further highlights the potential that exist in developing metal-based small molecules as anticancer drugs.

RESULTS

AuPhos-19 inhibits proliferation and induces apoptotic cell death in TNBC cells

AuPhos-19 (Figures 1A, S1, and S2) was identified as part of our research program to develop stable gold(III) compounds that target unique pathways of the mitochondria as probes or therapeutics. The compound is stabilized by cyclometalation and supported by σ-donating chiral quinoxaline phosphine ligand. The compound was synthesized and fully characterized as a monomeric gold compound (Kim et al., 2019). We evaluated the effect of AuPhos-19 on TNBC cell survival in a panel of TNBC (MDA-MB-468, MDA-MB-231, 4T1, and HCC1937) and the normal breast epithelial cell line (MCF-10A) using the MTT assay. AuPhos-19 demonstrated potent *in vitro* cytotoxic effect in a broad panel of TNBC cell lines that possess different histological subtypes including MDA-MB-468, MDA-MB-231, 4T1, HCC1937, MDA-MB-436, HS578T, and SUM 159 with IC_{50} values of 0.22, 0.56, 0.316, 0.65, 0.20, 0.21, and 0.28 μM, respectively after 72 h (Figures 1B and 1C). We observed a lesser cytotoxic effect in the normal breast cell line (MCF10-A) with IC_{50} of 1.62 μM. To further evaluate the anti-proliferative effect of AuPhos-19 on TNBC cells, we performed colony formation assay with MDA-MB-468 and 4T1 cells. Colony formation was significantly inhibited after treatment with AuPhos-19 for 10 days (Figure 1H).

We analyzed the effect of AuPhos-19 on cell cycle by flow cytometry. We observed a concentration-dependent increase in G0/G1 cell cycle population in MDA-MB-468 cells treated at 0.3 and 0.6 μM AuPhos-19 for

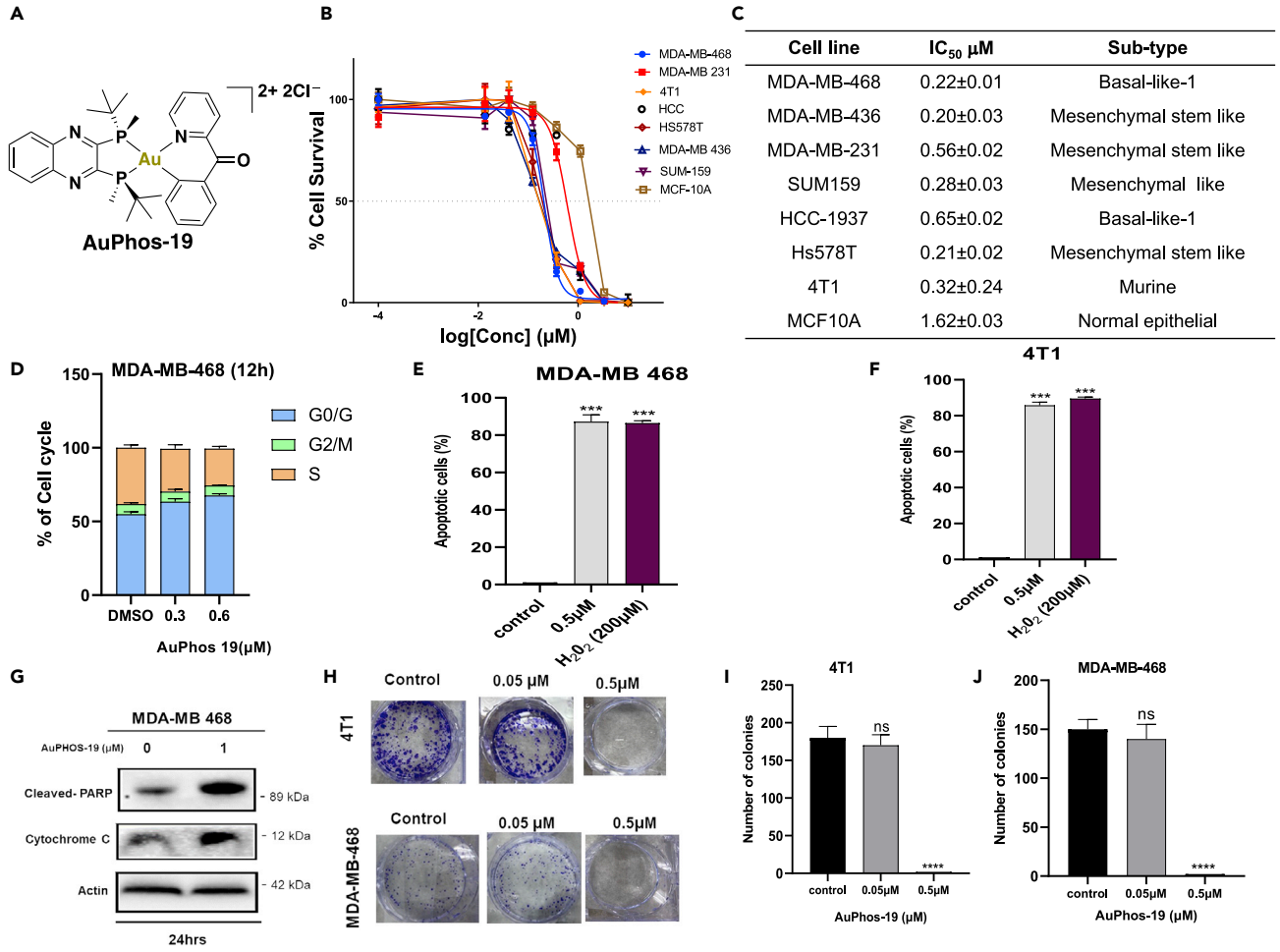

Figure 1. AuPhos-19 inhibits TNBC proliferation

(A) Chemical structure of AuPhos-19.

(B) Cell viability evaluated using MTT assay (C) Table of IC_{50}s extrapolated from dose-response curves with TNBC classification (Lehmann et al., 2011). Cells were exposed to increasing concentrations of AuPhos-19 over the course of 72 h. Mean ± SEM n = 3.

(D) Effect of AuPhos-19 on cell cycle distribution in TNBC cell line MDA-MB-468 after 12 h of treatment. Data are plotted as the mean ± SD (n = 3).

(E and F) Flow cytometry analyses of the apoptotic effect of AuPhos-19. n = 3.

(G) Western blot analyses of apoptosis-related proteins in TNBC cells treated with AuPhos-19 at the indicated concentration.

(H) Impact of AuPhos-19 on colony formation in TNBC cell lines (I) 4T1 and (J) MDA-MB-468 n = 3. Data are presented as mean ± SD. Data presented in E, F, I, and J were analyzed by ordinary one-way ANOVA followed by Dunnett's multiple comparison test (***p < 0.001, ****p < 0.0001. n.s. = not significant).

12 h. After 12 h, a 16% and 24% increase in the G1 cell population was observed at concentrations of 0.3 and 0.6 μM, respectively, compared to the control. Similar percent decrease in S-phase cell population for the respective treatment concentrations at the same period of 12 h was observed (Figures 1D and S13). This result suggests that AuPhos-19 arrests cell cycle at the G1-phase. We further investigated the effect of AuPhos-19 to induce apoptosis in TNBC. This assessment was done via flow cytometry analysis of MDA-MB-468 cells and 4T1 cells treated with 0.5 μM AuPhos-19 for 24 h. Results from the flow cytometry analysis showed that AuPhos-19 induced significant apoptosis in MDA-MB-468 cells with about 87% percent increase in apoptotic cells after treatment with 0.5 μM AuPhos-19 compared to control. We obtained a similar result in 4T1 cells under the same treatment conditions (Figures 1E, 1F, and S14). We subjected MDA-MB-468 cells treated with AuPhos-19 to immunoblotting analysis to assess the expression of key markers of apoptosis, cleaved PARP, and cytochrome *c*. Our result showed that AuPhos-19 significantly increased the expression of cleaved PARP after 24 h in MDA-MB-468 cells. Also, significant cytochrome *c* release in MDA-MB-468 cells treated with 1 μM AuPhos-19 for 24 h compared to control was observed. The cytochrome *c* causes activation of the apoptotic protease activating factor-1 (APAF-1) which in turn causes

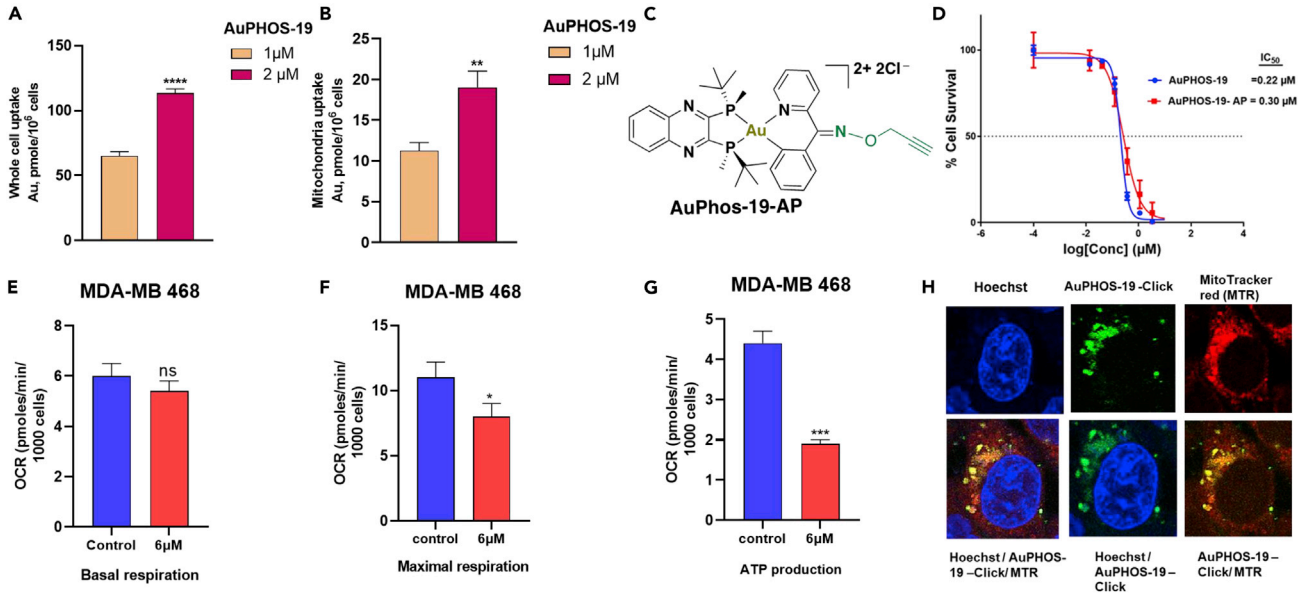

Figure 2. *In-vitro* localization of AuPhos-19

(A and B) Concentration dependent whole cell and mitochondria uptake of AuPhos-19 in MDA-MB-468 cells treated at the indicated concentrations for 18 h. Intracellular Au content was measured by GF-AAS. Data are presented as mean ± SEM (n = 3). Data were analyzed by two-tailed unpaired Student's *t* test (**p < 0.01, ****p < 0.0001).

(C) Chemical structure of clickable AuPhos-19 -alkyne probe (AP).

(D) Cell viability of MDA-MB-468 cells using the MTT assay after 72 h of treatment, comparing AuPhos-19 versus AuPhos-19 -AP. Data are plotted as the mean ± SEM (n = 3). IC_{50}, median inhibitory concentration.

(E–G) Extrapolated data from Mito stress test of MDA-MB-468 cells treated with AuPhos-19 -AP. Data are plotted as the mean ± SEM (n = 4). Data were analyzed by two-tailed unpaired Student's *t* test (*p < 0.05, ***p < 0.001, n.s. = not significant).

(H) AuPhos-19 -AP accumulation in the mitochondria of MDA-MB-468 cells visualized by confocal microscopy. Cells were treated at 20 μM for 1 h. Panels: i) Hoechst as the nuclear counterstain, ii) AuPhos-19 -AP – Alexa Fluor 488 azide adduct, iii) MitoTracker Red CM-H_2XRos (MTR) alone, iv) Merge of all three channels, v) Merge of Hoechst and AuPhos-19 -AP, vi) Merge of AuPhos-19 -AP -AP and MTR.

activation of caspase-9 (initiator caspase), caspase-3 (executioner caspase), and consequently apoptotic cell death (Chipuk et al., 2006; Garrido et al., 2006). This suggests that the mitochondria mediated apoptosis may contribute to the mechanism of cell death induced by AuPhos-19 in these TNBC cells.

AuPhos-19 accumulates in the mitochondria of TNBC cells

To gain insight into the mechanism of action (MOA) of AuPhos-19, we examined its accumulation and location in living cells. The cytotoxic effects of small molecules and their intracellular protein target engagement are attributed in part to the ability of the small molecule to penetrate the cell membrane. We confirmed whole cell uptake of the compound by measuring intracellular gold content in MDA-MB 468 cells exposed to AuPhos-19 for 18 h using the graphite furnace atomic absorption spectroscopy (GF-AAS). We further examined the accumulation of AuPhos-19 in mitochondria isolated from MDA-MB-468 cells via fractionation and found that the gold content detected using GF-AAS showed concentration-dependent accumulation of the compound in the mitochondria of cancer cells (Figures 2A and 2B). This accumulation in the mitochondria could be attributed to the lipophilic cationic character of AuPhos-19, which enables it to penetrate the lipid bilayers of the mitochondria membrane.

Localization studies involving AuPhos-19 in cancer cells was demonstrated by initial modification of AuPhos-19 to incorporate an alkyne handle, herein referred to as AuPhos-19 -alkyne-probe (AuPhos-19 -AP) to enable fluorescence visualization of the compound in the cells via click chemistry, specifically via copper-catalyzed azide-alkyne cycloaddition (CuACC) (Figures 2C, Scheme 1, and S15B) (Hong et al., 2010; Tyler et al., 2017; Wirth et al., 2015). A comparison of the effect of the clickable AuPhos-19 -AP with the parent molecule showed that it similarly inhibited the *in vitro* proliferation of MDA-MB-468 cells and decreased oxygen consumption rate assessed by the Mito stress test assay (Figures 2D–2G and S15A). We demonstrated the colocalization of AuPhos-19 -AP with a mitochondria-specific dye

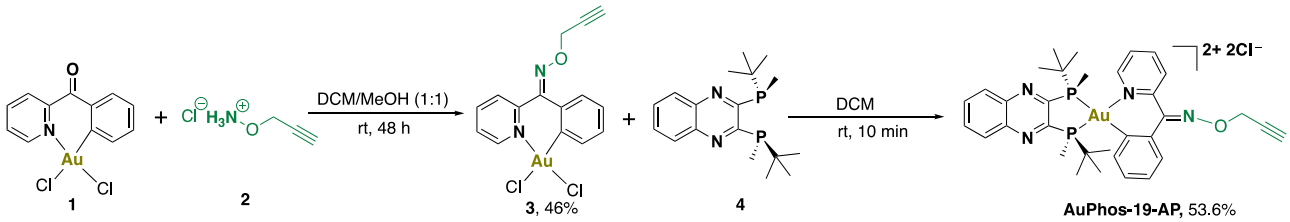

Scheme 1. Synthesis of alkyne-functionalized AuPhos-19 (AuPhos-19-AP) to investigate gold(III) complex localization

MitoTracker Red CM-H_2XRos (MTR), using fluorescence microscopy (Figures 2H and S15B). This verifies our preceding uptake data that show that AuPhos-19 accumulates in the mitochondria of the cancer cells.

AuPhos-19 disrupts metabolism in TNBC cells

TNBC is characterized by metabolic heterogeneity. To confirm the metabolic status of a panel of TNBC cells, we used the Seahorse XF analyzer to assess the oxygen consumption rate (OCR) and extracellular acidification rate (EACR) to gain insights into mitochondria function (OXPHOS) and glycolysis, respectively. We evaluated the ratio of OCR to ECAR to represent an index of preference for oxidative metabolism (OXPHOS) versus glycolysis in the TNBC cell lines (Lanning et al., 2017; Zhang et al., 2012). Through this functional assay, we showed that MDA-MB-468 and 4T1 cells had the highest dependence on oxidative metabolism than glycolysis among the four TNBC cell lines. MDA-MB-231 showed more dependence on glycolysis compared to other cell lines, HCC-1937 showed high OCR rates comparable to MDA-MB-468, 4T1 and high ECAR comparable to MDA-MB-231; however, the index of preference showed more dependence on oxidative metabolism for HCC-1937 (Figures 3A and 3D). These differences in metabolic phenotype correlate with the observed level of cytotoxic action of AuPhos-19; MDA-MB-468 and 4T1 were more sensitive to AuPhos-19 compared to the more glycolytic MDA-MB-231.

Given current understanding that functional mitochondrial is essential for the survival of cancer cells and that perturbation of mitochondrial processes may represent an effective approach to cancer treatment, we evaluated the effect of AuPhos-19 on mitochondrial bioenergetics in the cell lines using the Mito stress test assay to measure OCR. The evaluation involved a pneumatic injection of AuPhos-19 into wells containing adhered TNBC cells. This was followed by injection of known inhibitors of the electron transport chain (ETC) to measure specific parameters (Figure 3F). AuPhos-19 induced a dose-dependent decrease of mitochondrial maximal respiration and ATP production (Figures 3G–3I). The depletion of OCR by AuPhos-19 implies inhibition of mitochondrial respiration (OXPHOS) in TNBC.

Recent studies have shown the importance of the AMP-activated protein kinase (AMPK) to mitochondria health. As a sensor of low intracellular energy levels (ATP), AMPK mediates cellular response to mitochondrial assaults and energy depletion. Often, AMPK is activated in response to low energy levels (Herzig and Shaw, 2018). Also, it is known that downstream effects of AMPK activation include inhibition of the mammalian target of rapamycin (mTOR) which is important for growth and proliferation as well as inhibition of the acetyl CoA enzyme (ACC) needed for fatty acid synthesis (Herzig and Shaw, 2018; Luo et al., 2010). Our immunoblotting analysis showed AMPK activation in response to OXPHOS inhibition by AuPhos-19 in MDA-MB-468 and MDA-MB-231 cells. We also observed significant decrease in mTOR expression and inhibition of ACC after 24 h exposure to AuPhos-19 (1 μM) (Figure 3J). Taken together, AuPhos-19 interferes with the metabolic profile of TNBC.

AuPhos-19 induces mitochondria dysfunction

To further examine the effect of AuPhos-19 on mitochondria function, we evaluated its effect on mitochondrial membrane potential (MMP). We measured MMP using the JC-1 dye by which AuPhos-19 strongly depolarizes MMP in MDA-MB-468 and MDA-MB-231 cells exposed to compound over a short period of time compared to untreated control cells (Figures 4A, 4B, and S16). This result indicates that the mitochondria OXPHOS may be a target for AuPhos-19.

ROS production is elevated in tumor cells due to their higher metabolic rate and hypoxia compared to normal cells. However, to maintain tumor progression, these transformed cells have increased antioxidant

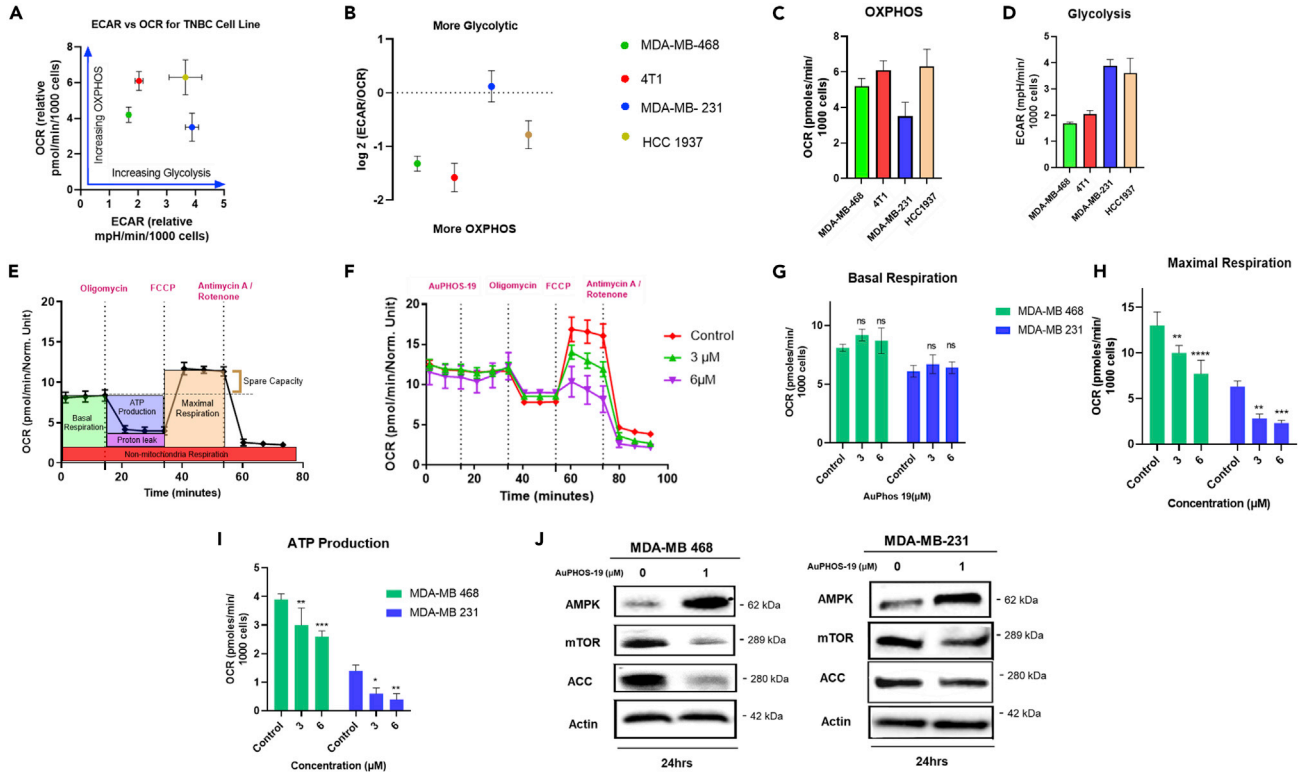

Figure 3. AuPhos-19 inhibits oxygen consumption in TNBC

(A) ECAR vs OCR extrapolated from seahorse metabolism analysis. Mean ± SEM (n = 3).

(B) Index of metabolic dependence on OXPHOS and glycolysis.

(C and D) Bar graphs showing OCR and ECAR readings extrapolated from seahorse metabolism analysis represented in A and B.

(E) Schematic representation of the Seahorse mitochondrial respiration experiment.

(F) Seahorse bioenergetic stress test of AuPhos-19 in MDA-MB-468. Normalization of OCR was done per 1,000 cells. Data are plotted as the mean ± SEM, n = 4.

(G–I) Extrapolated data from Mito stress test of MDA-MB-468 and MDA-MB-231 cells treated with AuPhos-19. Data are plotted as the mean ± SEM (n = 4). Data were analyzed by two-way ANOVA followed by Dunnett's multiple comparison test (*$p < 0.05$, **$p < 0.01$, ***$p < 0.001$, ****$p < 0.0001$. n.s. = not significant).

(J) Western blot analyses of proteins associated with the AMPK pathway. TNBC cells were treated with AuPhos-19 (1µM) for 24 h.

pathways to attenuate the ROS-induced oxidative stress. Given that ROS can trigger programmed cell death, several studies in recent years have explored ROS-induced oxidative damage as a therapeutic approach to kill cancer cells (Perillo et al., 2020; Totten et al., 2021). Depolarization of the mitochondria membrane potential is related to production of mitochondria reactive oxygen species (mtROS) (Sundqvist et al., 2017; Vyssokikh et al., 2020; Zorov et al., 2014). Given that AuPhos-19 induced significant depolarization of the MMP, we used the mitochondria-specific MitoSOX red dye (excitation/emission wavelength of 510/580 nm) to evaluate mitochondria superoxide production in MDA-MB-231 and MDA-MB-468 cells exposed to AuPhos-19. The MitoSOX dye is oxidized in the mitochondria of living cells by superoxide to form a highly fluorescent product (Sundqvist et al., 2017). We exposed the MDA-MB-468 and MDA-MB-231 cells to AuPhos-19 (2 µM) and quantified the intensity of the MitoSOX staining in the cells via flow cytometry analysis. After 90 min of treatment, we observed significant increase in mtROS (greater MitoSOX fluorescence intensity) compared to the control (Figures 4C and 4D). To confirm our observation that AuPhos-19 induces mtROS production in the TNBC cells, we pre-treated these cells with Mitotempo (2 µM) for 1 h before introducing our compound. Mitotempo is a mitochondria-targeted antioxidant that attenuates superoxide radicals (Yang et al., 2018). As shown in (Figures 4C and 4D), pre-treatment with Mitotempo reduced the generation of mtROS compared to treatment with AuPhos-19 2 µM only.

Given the perturbations of mitochondria function caused by AuPhos-19, we sought to further examine the consequence of these mitochondria insults. The proximal location of the mtDNA to the respiratory chain

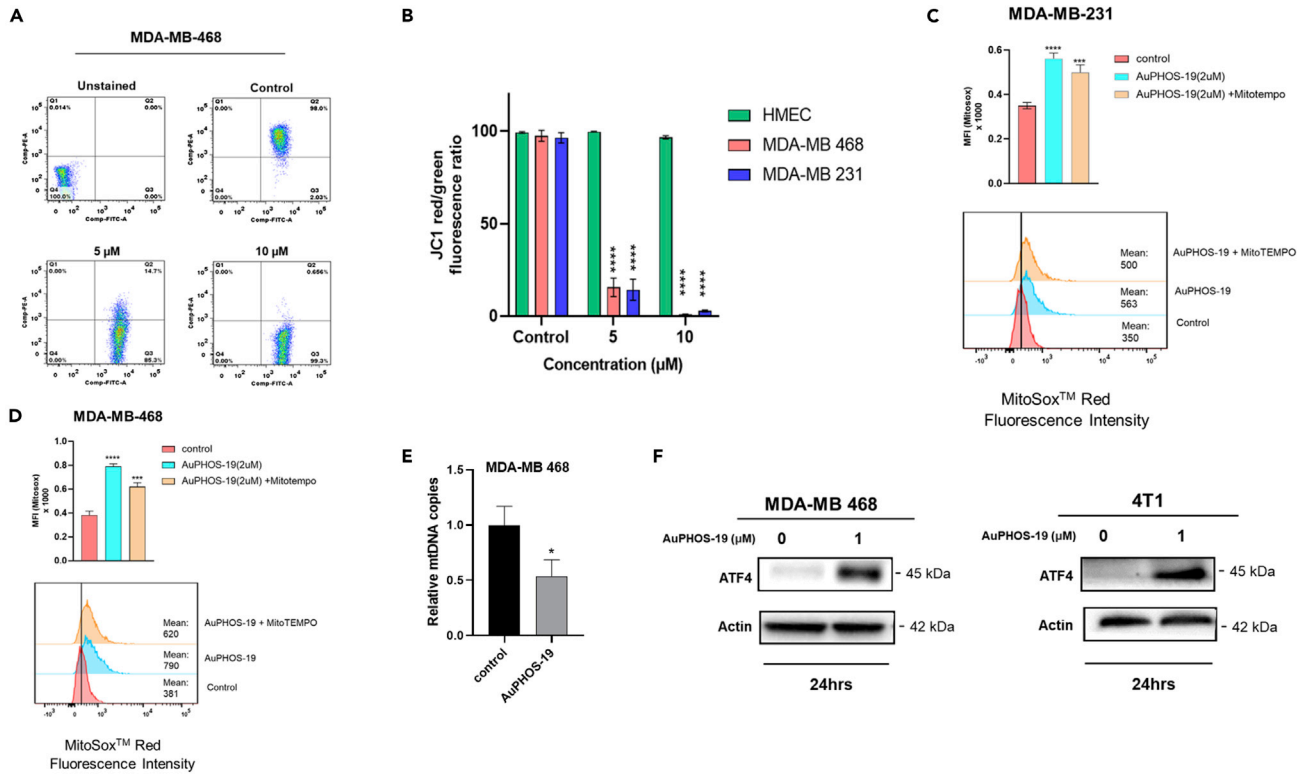

Figure 4. AuPhos-19 perturbs mitochondria function

(A) Mitochondria membrane potential performed using the JC-1 assay and analyzed by FACS of MDA-MB-468 cells.

(B) Bar graph showing loss of PE fluorescence (J-aggregates) in comparison to the control. Data are plotted as the mean ± SD (n = 3). Data were analyzed by two-way ANOVA followed by Dunnett's multiple comparison test (****$p < 0.0001$).

(C and D) mtROS measured by MitoSOX (PE channel). Data are plotted as the mean ± SD (n = 3). Data were analyzed by ordinary one-way ANOVA followed by Dunnett's multiple comparison test (***$p < 0.001$, ****$p < 0.0001$).

(E) Relative mtDNA levels in MDA-MB-468 cells. Mean ± SD (n = 3). Data analyzed by two-tailed unpaired Student's *t* test (*$p < 0.05$).

(F) Western blot analyses showing ATF4 activation in TNBC cells treated with AuPhos-19 (1μM) for 24 h.

makes it susceptible to mtROS-induced damage or depletion (Ide et al., 2001; Scheibye-Knudsen et al., 2015; Shadel and Horvath, 2015). Depletion of the mtDNA or decrease in the mitochondria copy number causes changes in the expression of important mitochondria proteins like TWINKLE and POLG which are necessary for mtDNA replication (Ide et al., 2001; Pokrzywinski et al., 2016). We measured mitochondria DNA copy number in MDA-MB-468 cells treated with AuPhos-19 (1μM) to examine mtDNA damage (Djeungoue-Petga et al., 2019; Quiros et al., 2017). Our data showed that AuPhos-19 significantly reduced mtDNA copy number (Figure 4E). Immunoblotting of the activating transcription factor 4 (ATF4), a transcription factor that is activated in response to mitochondria stress and mediated by the integrated stress response pathway (Kasai et al., 2018), showed strong ATF4 activation in TNBC cells treated with AuPhos-19 (Figure 4F). These findings further indicate that AuPhos-19 disrupts mitochondria processes as a mechanism of action in TNBC (Ide et al., 2001; Scheibye-Knudsen et al., 2015; Shadel and Horvath, 2015).

AuPhos-19 inhibits *in vivo* TNBC tumor progression

The ability of AuPhos-19 to induce TNBC-selective mitochondrial dysfunction inspired preliminary exploration of its potential to inhibit tumor growth *in vivo*. Modulators of mitochondrial metabolism are an emerging strategy and are attractive anticancer agents, with immense potential for effective combination therapy against aggressive tumors. AuPhos-19 displays potent activity in TNBC cells with selectivity over normal breast epithelial cells, thus it is a suitable compound to assess *in vivo*. We examined the *in vivo* effect of AuPhos-19 on tumor progression in 4T1-iRFP xenograft tumor mouse model (Figures 5A and 5B). We administered either vehicle or AuPhos-19 three times a week via intraperitoneal (IP) injection at a dose equivalent of 10 mg/kg for 16 days. Measurements of tumor volume indicated a 55% tumor growth

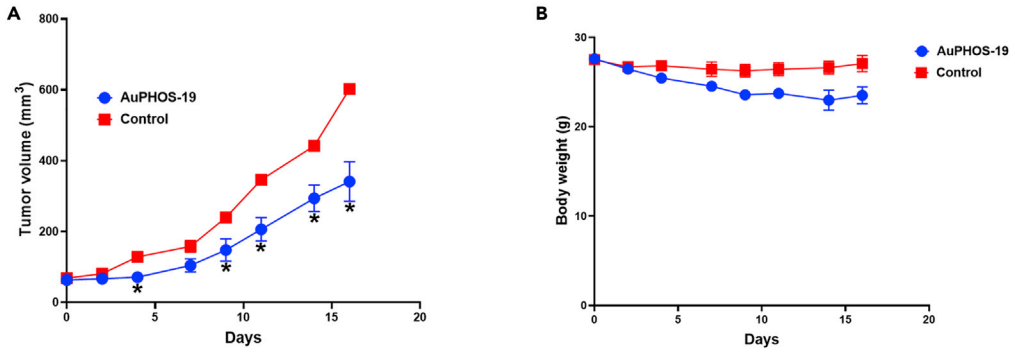

Figure 5. *In vivo* anticancer potential of AuPhos-19

(A) AuPhos-19 inhibits subcutaneous 4T1-iRFP tumor growth in immunocompromised NSG mice as measured by tumor volume.

(B) The mice body weight of AuPhos-19 -treated mice and vehicle control. AuPhos-19 was administered intraperitoneally at 10 mg/kg, thrice a week, six doses (n = 4 mice per group). Data represent the mean ± SEM Two-sided Student's *t* test, p values are relative to vehicle control; * $0.01 \leq p < 0.05$.

retardation in compound-treated NSG compared to vehicle-treated mice. Optimization of AuPhos-19 will likely improve the *in vivo* efficacy. Additionally, a reduction in mice body weight was observed for AuPhos-19 -treated mice, which can be alleviated with an optimized candidate—an ongoing enterprise in our lab. Overall, our data suggest that AuPhos-19 is a potent gold(III) agent with promise as an anticancer agent against TNBC *in vivo*.

DISCUSSION

Over the past two decades, there have been significant advancements in the treatment of breast cancer and improved survival rate; however, the highly aggressive and metastatic TNBC remains an unsolved problem as the overall survival rate for women with this breast cancer subtype remains poor. TNBCs lack the expression of progesterone, estrogen, and Her2 receptors hence they cannot be treated with the targeted therapy used to treat other breast cancer subtypes. Chemotherapy remains the main treatment option for patients with TNBC; however, tumor relapse after treatment and chemotherapy resistance poses a serious clinical challenge. Hence, there is an urgent need for more effective drugs/regimens for the treatment of TNBC. In the past few years, the potential of organometallic chemistry has been greatly explored to develop different metal-based small molecules as anticancer drugs against TNBCs.

Previous work from our laboratory have led to the development of gold-based small molecules with potent anticancer activity against different cancer cells (Arojojoye et al., 2020; Kim et al., 2021; Mertens et al., 2020). Preliminary cellular response evoked by AuPhos-19 was differentiated from the other gold(I) compounds tested in our previous report. Specifically, DNA damage response markers such as γH2AX and cleaved PARP were significantly elevated, indicative of a stress condition induced by AuPhos-19. Additionally, the potential for facile functionalization toward mechanistic studies, numerous sites for chemical modification including the quinoxaline framework, substituents on the phosphine donors, and the cyclometalated ligands for an improved AuPhos-19 was the premise for a thorough mechanistic investigation. Herein, we report the results of our studies with a Au(III) complex AuPhos-19, which we found to be potent against a panel of triple-negative breast cancer cells (MDA-MB-468, MDA-MB-231, 4T1, HCC, HS578T, MDA-MB-436, and SUM 159). We hypothesized that the lipophilic cation character of AuPhos-19 will facilitate its accumulation in the mitochondria due to the well-established negative redox potential of the mitochondria of cancer cells to induce stress-related apoptosis. The phosphine donor ligand imparts chirality, lipophilicity, and a di-cationic state to AuPhos-19, which are important chemical properties for mitochondria drug discovery. A unique feature of AuPhos-19 is the labile Au-N(sp2) bond, which may act as a coordination site for protein binding and modulation. We envisioned these properties of AuPhos-19 as crucial for further development. Future target identification studies using biotinylated probes would shed more light on mitochondrial protein targets.

In the 1920s, Otto Warburg described his observation that cancer cells have high glucose utilization and high lactate secretion even in the presence of oxygen; this led to the assumption that mitochondria

metabolism is impaired in cancer cells. However, research over the past few decades has led to the understanding that the mitochondria are functional in cancer cells to produce energy (ATP) via oxidative phosphorylation (OXPHOS) needed to support tumorigenesis. In fact, studies have shown a positive correlation between OXPHOS activity and metastatic potential in primary breast cancer cells (Lehuédé et al., 2016). In addition, metabolic reprogramming is well accepted now as a hallmark of cancer and provides new approach to overcome TNBC and other forms of malignancy (Hanahan and Weinberg, 2011).

We demonstrated that AuPhos-19 accumulates in the mitochondria of TNBC and inhibits proliferation by inducing cell cycle arrest and apoptotic cell death. These observations could be due to depletion of ATP levels which lead to the activation of AMPK. AMPK serves as an indicator for energy levels and is activated upon shortage of energy (Luo et al., 2010). Treatment of the TNBC cell lines with AuPhos-19 causes AMPK activation by inhibiting mitochondria respiration (OXPHOS). Consistent with current understanding that AMPK activation leads to the regulation of different downstream targets associated with metabolic processes, AuPhos-19 caused significant depletion of mTOR. mTOR signaling is regularly activated in tumors to maintain survival and drive proliferation (Zou et al., 2020). Furthermore, AuPhos-19-induced AMPK activation led to ACC inhibition. ACC is a rate-limiting enzyme for fatty acid synthesis and is essential for tumorigenesis (Luo et al., 2010).

Mitochondria dysfunctions induced by treatment of TNBC cells with AuPhos-19 include mitochondria membrane depolarization, mtROS production, as well as mtDNA depletion. Interestingly, mitochondria perturbation in TNBC cells by AuPhos-19 was further confirmed by strong activation of ATF4. In addition, AuPhos-19 showed modest antitumor activity as a single agent *in vivo* in a metastatic 4T1 TNBC murine model engineered to express RFP.

In summary, our *in vitro* and *in vivo* data show AuPhos-19 as a potential candidate for the treatment of TNBC and further highlights the potential in exploring the development gold-based small molecules for cancer treatment.

Limitations of the study

Although AuPhos-19 demonstrated high efficacy across different TNBC subtype *in vitro*, it showed modest potency *in vivo*. Future studies will be focused on optimization of this compound for improved *in vivo* efficacy in addition to target identification studies that will help identify direct protein targets of AuPhos-19.

STAR★METHODS

Detailed methods are provided in the online version of this paper and include the following:

- KEY RESOURCES TABLE
- RESOURCE AVAILABILITY
  - Lead contact
  - Materials availability
  - Data and code availability
- EXPERIMENTAL MODELS AND SUBJECT DETAILS
  - Cell culture
  - *In vivo* animal studies
- METHOD DETAILS
  - Chemistry
  - Cell viability assay
  - Apoptosis analysis
  - Immunoblotting
  - Cell cycle
  - Whole-cell uptake studies
  - Mitochondrial uptake assay
  - Colony formation assay
  - Bioenergetics measurement with seahorse XF96 analysis
  - Fluorescence visualization of AuPhos-19 compound in cells
  - Assessment of mitochondria DNA levels
  - Mitochondria membrane potential (JC1 assay)

- Mitochondria ROS (mtROS)
- *In vivo* experiment of AuPhos-19

- QUANTIFICATION AND STATISTICAL ANALYSIS

SUPPLEMENTAL INFORMATION

Supplemental information can be found online at https://doi.org/10.1016/j.isci.2022.104340.

ACKNOWLEDGMENTS

We thank all the core facilities at the University of Kentucky who provided support in completion of the experiments detailed in this manuscript. Specifically, the UK NMR Center supported by NSF (CHE-997738) and the flow cytometry and immune function core supported by the Office of the Vice President of Research, the Markey Cancer Center, and NCI Center Core Support Grant (P30 CA177558), and the microscopy facilities (UK Light Microscopy Core) for their assistance. We thank Dr. Kathleen O'Connor for generously providing us with some TNBC cell lines for this study. We thank Dr. Tomoko Sengoku PhD and Mr. Michael Alstott for their support with our redox metabolism experiments, supported by the shared resource(s) of the University of Kentucky Markey Cancer Center (P30CA177558). The University of Colorado, Boulder, supported by NIH S10RR026641 where the Waters Synapt G2 was used for high-resolution mass spectrometry. This work was funded by National Institutes of Health/NCI grant R01CA258421-01 (S.G.A.).

AUTHOR CONTRIBUTIONS

S.G.A. conceptualized the project. C.N.O. led the project and performed most of the experiments. C.N.O., S.O., and S.G., worked on synthetic modification of parent compound used in this study. C.N.O., J.H.K., and S.O. carried out animal studies. C.N.O. and R.T.M performed flow cytometry and confocal microscopy experiments. C.N.O. wrote the manuscript with guidance from S.G.A. S.G.A. revised the manuscript before submission.

DECLARATION OF INTERESTS

The authors declare the following financial interests/personal relationships which may be considered as potential competing interests: Samuel G. Awuah reports financial support was provided by University of Kentucky. Samuel G. Awuah reports a relationship with University of Kentucky that includes: funding grants. Samuel G. Awuah has patents pending to University of Kentucky Research Foundation.

Received: January 5, 2022
Revised: March 14, 2022
Accepted: April 27, 2022
Published: May 20, 2022

REFERENCES

Arojojoye, A.S., Mertens, R.T., Ofori, S., Parkin, S.R., and Awuah, S.G. (2020). Synthesis, characterization, and antiproliferative activity of novel chiral [QuinoxP* AuCl2]+ complexes. Molecules *25*, 5735. https://doi.org/10.3390/molecules25235735.

Ashton, T.M., McKenna, W.G., Kunz-Schughart, L.A., and Higgins, G.S. (2018). Oxidative phosphorylation as an emerging target in cancer therapy. Clin. Cancer Res. *24*, 2482–2490. https://doi.org/10.1158/1078-0432.ccr-17-3070.

Barnard, P.J., and Berners-Price, S.J. (2007). Targeting the mitochondrial cell death pathway with gold compounds. Coord. Chem. Rev. *251*, 1889–1902. https://doi.org/10.1016/j.ccr.2007.04.006.

Chipuk, J.E., Bouchier-Hayes, L., and Green, D.R. (2006). Mitochondrial outer membrane permeabilization during apoptosis: the innocent bystander scenario. Cell Death Differ. *13*, 1396–1402. https://doi.org/10.1038/sj.cdd.4401963.

Cimino, G.D., Pan, C.-X., and Henderson, P.T. (2013). Personalized medicine for targeted and platinum-based chemotherapy of lung and bladder cancer. Bioanalysis *5*, 369–391. https://doi.org/10.4155/bio.12.325.

Dawson, S., Provenzano, E., and Caldas, C. (2009). Triple negative breast cancers: clinical and prognostic implications. Eur. J. Cancer *45*, 27–40. https://doi.org/10.1016/s0959-8049(09)70013-9.

Djeungoue-Petga, M.A., Lurette, O., Jean, S., Hamel-Cote, G., Martin-Jimenez, R., Bou, M., Cannich, A., Roy, P., and Hebert-Chatelain, E. (2019). Intramitochondrial Src kinase links mitochondrial dysfunctions and aggressiveness of breast cancer cells. Cell Death Dis. *10*, 940. https://doi.org/10.1038/s41419-019-2134-8.

Garrido, C., Galluzzi, L., Brunet, M., Puig, P.E., Didelot, C., and Kroemer, G. (2006). Mechanisms of cytochrome c release from mitochondria. Cell Death Differ. *13*, 1423–1433. https://doi.org/10.1038/sj.cdd.4401950.

Hanahan, D., and Weinberg, R.A. (2011). Hallmarks of cancer: the next generation. Cell *144*, 646–674. https://doi.org/10.1016/j.cell.2011.02.013.

Herzig, S., and Shaw, R.J. (2018). AMPK: guardian of metabolism and mitochondrial homeostasis. Nat. Rev. Mol. Cell Biol. *19*, 121–135. https://doi.org/10.1096/fasebj.2018.32.1_supplement.379.3.

Hong, V., Steinmetz, N.F., Manchester, M., and Finn, M.G. (2010). Labeling live cells by copper-catalyzed alkyne– azide click chemistry. Bioconjug. Chem. *21*, 1912–1916. https://doi.org/10.1021/bc100272z.

Hudis, C.A., and Gianni, L. (2011). Triple-negative breast cancer: an unmet medical need. Oncologist *16*, 1–11. https://doi.org/10.1634/theoncologist.2011-s1-01.

Ide, T., Tsutsui, H., Hayashidani, S., Kang, D., Suematsu, N., Nakamura, K.-i., Utsumi, H., Hamasaki, N., and Takeshita, A. (2001). Mitochondrial DNA damage and dysfunction associated with oxidative stress in failing hearts after myocardial infarction. Circ. Res. *88*, 529–535. https://doi.org/10.1161/01.res.88.5.529.

Kasai, S., Yamazaki, H., Tanji, K., Engler, M.J., Matsumiya, T., and Itoh, K. (2018). Role of the ISR-ATF4 pathway and its cross talk with Nrf2 in mitochondrial quality control. J. Clin. Biochem. Nutr. *64*, 1–12.

Kelland, L. (2007). The resurgence of platinum-based cancer chemotherapy. Nat. Rev. Cancer *7*, 573–584. https://doi.org/10.1038/nrc2167.

Kim, J., and DeBerardinis, R.J. (2019). Mechanisms and implications of metabolic heterogeneity in cancer. Cell Metab. *30*, 434–446. https://doi.org/10.1016/j.cmet.2019.08.013.

Kim, J.H., Ofori, S., Parkin, S., Vekaria, H., Sullivan, P.G., and Awuah, S.G. (2021). Anticancer gold (III)-bisphosphine complex alters the mitochondrial electron transport chain to induce *in vivo* tumor inhibition. Chem. Sci. *12*, 7467–7479. https://doi.org/10.1039/d1sc01418h.

Kim, J.H., Reeder, E., Parkin, S., and Awuah, S.G. (2019). Gold(I/III)-phosphine complexes as potent antiproliferative agents. Sci. Rep. *9*, 12335. https://doi.org/10.1038/s41598-019-48584-5.

Lanning, N.J., Castle, J.P., Singh, S.J., Leon, A.N., Tovar, E.A., Sanghera, A., MacKeigan, J.P., Filipp, F.V., and Graveel, C.R. (2017). Metabolic profiling of triple-negative breast cancer cells reveals metabolic vulnerabilities. Cancer Metab. *5*, 6. https://doi.org/10.1186/s40170-017-0168-x.

Lehmann, B.D., Bauer, J.A., Chen, X., Sanders, M.E., Chakravarthy, A.B., Shyr, Y., and Pietenpol, J.A. (2011). Identification of human triple-negative breast cancer subtypes and preclinical models for selection of targeted therapies. J. Clin. Invest. *121*, 2750–2767. https://doi.org/10.1172/JCI45014.

Lehuédé, C., Dupuy, F., Rabinovitch, R., Jones, R.G., and Siegel, P.M. (2016). Metabolic plasticity as a determinant of tumor growth and metastasis. Cancer Res. *76*, 5201–5208. https://doi.org/10.1158/0008-5472.can-16-0266.

Lin, N.U., Vanderplas, A., Hughes, M.E., Theriault, R.L., Edge, S.B., Wong, Y.N., Blayney, D.W., Niland, J.C., Winer, E.P., and Weeks, J.C. (2012). Clinicopathologic features, patterns of recurrence, and survival among women with triple-negative breast cancer in the National Comprehensive Cancer Network. Cancer *118*, 5463–5472. https://doi.org/10.1002/cncr.27581.

Luo, Z., Zang, M., and Guo, W. (2010). AMPK as a metabolic tumor suppressor: control of metabolism and cell growth. Future Oncol. *6*, 457–470. https://doi.org/10.2217/fon.09.174.

Masoud, R., Reyes-Castellanos, G., Lac, S., Garcia, J., Dou, S., Shintu, L., Abdel Hadi, N., Gicquel, T., El Kaoutari, A., Diémé, B., et al. (2020). Targeting mitochondrial complex I overcomes chemoresistance in high oxphos pancreatic cancer. Cell Rep. Med. *1*, 100143. https://doi.org/10.1016/j.xcrm.2020.100143.

Mertens, R.T., Parkin, S., and Awuah, S.G. (2020). Cancer cell-selective modulation of mitochondrial respiration and metabolism by potent organogold (iii) dithiocarbamates. Chem. Sci. *11*, 10465–10482. https://doi.org/10.1039/d0sc03628e.

Milacic, V., and Dou, Q.P. (2009). The tumor proteasome as a novel target for gold (III) complexes: implications for breast cancer therapy. Coord. Chem. Rev. *253*, 1649–1660. https://doi.org/10.1016/j.ccr.2009.01.032.

Nardon, C., Boscutti, G., and Fregona, D. (2014). Beyond platinums: gold complexes as anticancer agents. Anticancer Res. *34*, 487–492.

Ndagi, U., Mhlongo, N., and Soliman, M.E. (2017). Metal complexes in cancer therapy – an update from drug design perspective. Drug Des. Dev. Ther. *11*, 599–616. https://doi.org/10.2147/dddt.s119488.

Ortega, E., Zamora, A., Basu, U., Lippmann, P., Rodríguez, V., Janiak, C., Ott, I., and Ruiz, J. (2020). An Erlotinib gold(I) conjugate for combating triple-negative breast cancer. J. Inorg. Biochem. *203*, 110910. https://doi.org/10.1016/j.jinorgbio.2019.110910.

Pelicano, H., Zhang, W., Liu, J., Hammoudi, N., Dai, J., Xu, R.-H., Pusztai, L., and Huang, P. (2014). Mitochondrial dysfunction in some triple-negative breast cancer cell lines: role of mTOR pathway and therapeutic potential. Breast Cancer Res. *16*, 434. https://doi.org/10.1186/s13058-014-0434-6.

Perillo, B., Di Donato, M., Pezone, A., Di Zazzo, E., Giovannelli, P., Galasso, G., Castoria, G., Migliaccio, A.J.E., and Medicine, M. (2020). ROS in cancer therapy: the bright side of the moon. Exp. Mol. Med. *52*, 192–203. https://doi.org/10.1038/s12276-020-0384-2.

Pokrzywinski, K.L., Biel, T.G., Kryndushkin, D., and Rao, V.A. (2016). Therapeutic targeting of the mitochondria initiates excessive superoxide production and mitochondrial depolarization causing decreased mtDNA integrity. PLoS One *11*, e0168283. https://doi.org/10.1371/journal.pone.0168283.

Quiros, P.M., Goyal, A., Jha, P., and Auwerx, J. (2017). Analysis of mtDNA/nDNA ratio in mice. Curr. Protoc. Mouse Biol. *7*, 47–54. https://doi.org/10.1002/cpmo.21.

Rackham, O., Nichols, S.J., Leedman, P.J., Berners-Price, S.J., and Filipovska, A. (2007). A gold (I) phosphine complex selectively induces apoptosis in breast cancer cells: implications for anticancer therapeutics targeted to mitochondria. Biochem. Pharmacol. *74*, 992–1002. https://doi.org/10.1016/j.bcp.2007.07.022.

Raninga, P.V., Lee, A., Sinha, D., Dong, L.-f., Datta, K.K., Lu, X., Kalita-de Croft, P., Dutt, M., Hill, M., Pouliot, N., et al. (2020). Marizomib suppresses triple-negative breast cancer via proteasome and oxidative phosphorylation inhibition. Theranostics *10*, 5259–5275. https://doi.org/10.7150/thno.42705.

Pia Rigobello, M., Messori, L., Marcon, G., Agostina Cinellu, M., Bragadin, M., Folda, A., Scutari, G., and Bindoli, A. (2004). Gold complexes inhibit mitochondrial thioredoxin reductase: consequences on mitochondrial functions. J. Inorg. Biochem. *98*, 1634–1641. https://doi.org/10.1016/j.jinorgbio.2004.04.020.

Rindfleisch, J.A., and Muller, D. (2005). Diagnosis and management of rheumatoid arthritis. Am. Fam. Physician *72*, 1037–1047.

Sancho, P., Barneda, D., and Heeschen, C. (2016). Hallmarks of cancer stem cell metabolism. Br. J. Cancer *114*, 1305–1312. https://doi.org/10.1038/bjc.2016.152.

Scheibye-Knudsen, M., Fang, E.F., Croteau, D.L., Wilson, D.M., III, and Bohr, V.A. (2015). Protecting the mitochondrial powerhouse. Trends Cell Biol. *25*, 158–170. https://doi.org/10.1016/j.tcb.2014.11.002.

Shadel, G.S., and Horvath, T.L. (2015). Mitochondrial ROS signaling in organismal homeostasis. Cell *163*, 560–569. https://doi.org/10.1016/j.cell.2015.10.001.

Shi, Y., Lim, S.K., Liang, Q., Iyer, S.V., Wang, H.-Y., Wang, Z., Xie, X., Sun, D., Chen, Y.-J., Tabar, V., et al. (2019). Gboxin is an oxidative phosphorylation inhibitor that targets glioblastoma. Nature *567*, 341–346. https://doi.org/10.1038/s41586-019-0993-x.

Sundqvist, M., Christenson, K., Björnsdottir, H., Osla, V., Karlsson, A., Dahlgren, C., Speert, D.P., Fasth, A., Brown, K.L., and Bylund, J. (2017). Elevated mitochondrial reactive oxygen species and cellular redox imbalance in human NADPH-oxidase-deficient phagocytes. Front. Immunol. *8*, 1828. https://doi.org/10.3389/fimmu.2017.01828.

Totten, S.P., Im, Y.K., Cepeda Cañedo, E., Najyb, O., Nguyen, A., Hébert, S., Ahn, R., Lewis, K., Lebeau, B., La Selva, R., et al. (2021). STAT1 potentiates oxidative stress revealing a targetable vulnerability that increases phenformin efficacy in breast cancer. Nat. Commun. *12*, 3299–3320. https://doi.org/10.1038/s41467-021-23396-2.

Tyler, D.S., Vappiani, J., Caneque, T., Lam, E.Y.N., Ward, A., Gilan, O., Chan, Y.C., Hienzsch, A., Rutkowska, A., Werner, T., et al. (2017). Click chemistry enables preclinical evaluation of targeted epigenetic therapies. Science *356*, 1397–1401. https://doi.org/10.1126/science.aal2066.

Urra, F.A., Muñoz, F., Córdova-Delgado, M., Ramírez, M.P., Peña-Ahumada, B., Rios, M., Cruz, P., Ahumada-Castro, U., Bustos, G., Silva-Pavez, E., et al. (2018). FR58P1a; a new uncoupler of OXPHOS that inhibits migration in triple-negative breast cancer cells via Sirt1/AMPK/β1-integrin pathway. Sci. Rep. *8*, 13190. https://doi.org/10.1038/s41598-018-31367-9.

Vyssokikh, M.Y., Holtze, S., Averina, O.A., Lyamzaev, K.G., Panteleeva, A.A., Marey, M.V., Zinovkin, R.A., Severin, F.F., Skulachev, M.V., Fasel, N., et al. (2020). Mild depolarization of the inner mitochondrial membrane is a crucial component of an anti-aging program. Proc. Natl. Acad. Sci. U S A *117*, 6491–6501. https://doi.org/10.1073/pnas.1916414117.

Warburg, O. (1956). On the origin of cancer cells. Science *123*, 309–314. https://doi.org/10.1126/science.123.3191.309.

Weinberg, S.E., and Chandel, N.S. (2015). Targeting mitochondria metabolism for cancer therapy. Nat. Chem. Biol. *11*, 9–15. https://doi.org/10.1038/nchembio.1712.

Wirth, R., White, J.D., Moghaddam, A.D., Ginzburg, A.L., Zakharov, L.N., Haley, M.M., and DeRose, V.J. (2015). Azide vs alkyne functionalization in Pt(II) complexes for post-treatment click modification: solid-state structure, fluorescent labeling, and cellular fate. J. Am. Chem. Soc. *137*, 15169–15175. https://doi.org/10.1021/jacs.5b09108.

Yang, S.-G., Park, H.-J., Kim, J.-W., Jung, J.-M., Kim, M.-J., Jegal, H.-G., Kim, I.-S., Kang, M.-J., Wee, G., Yang, H.-Y., et al. (2018). Mito-TEMPO improves development competence by reducing superoxide in preimplantation porcine embryos. Sci. Rep. *8*, 10130. https://doi.org/10.1038/s41598-018-28497-5.

Yeo, C.I., Ooi, K.K., and Tiekink, E.R. (2018). Gold-based medicine: a paradigm shift in anti-cancer therapy. Molecules *23*, 1410. https://doi.org/10.3390/molecules23061410.

Zhang, J., Nuebel, E., Wisidagama, D.R.R., Setoguchi, K., Hong, J.S., Van Horn, C.M., Imam, S.S., Vergnes, L., Malone, C.S., Koehler, C.M., and Teitell, M.A. (2012). Measuring energy metabolism in cultured cells, including human pluripotent stem cells and differentiated cells. Nat. Protoc. *7*, 1068–1085. https://doi.org/10.1038/nprot.2012.048.

Zorov, D.B., Juhaszova, M., and Sollott, S.J. (2014). Mitochondrial reactive oxygen species (ROS) and ROS-induced ROS release. Physiol. Rev. *94*, 909–950. https://doi.org/10.1152/physrev.00026.2013.

Zou, T., Lum, C.T., Lok, C.-N., Zhang, J.-J., and Che, C.-M. (2015). Chemical biology of anticancer gold (III) and gold (I) complexes. Chem. Soc. Rev. *44*, 8786–8801. https://doi.org/10.1039/c5cs00132c.

Zou, T., Zhang, J.J., Cao, B., Tong, K.C., Lok, C.N., and Che, C.M. (2016). Deubiquitinases as anticancer targets of gold complexes. Isr. J. Chem. *56*, 825–833. https://doi.org/10.1002/ijch.201600044.

Zou, Z., Tao, T., Li, H., and Zhu, X. (2020). mTOR signaling pathway and mTOR inhibitors in cancer: progress and challenges. Cell Biosci. *10*, 31. https://doi.org/10.1186/s13578-020-00396-1.

STAR★METHODS

KEY RESOURCES TABLE

REAGENT or RESOURCE	SOURCE	IDENTIFIER
Antibodies		
AMPKα	Cell Signaling Technology	Cat# 2532S; RRID: AB_330331
ACC	Cell Signaling Technology	Cat# 3662S; RRID: AB_2219400
mTOR	Cell Signaling Technology	Cat# 2972S; RRID: AB_330978
Cleaved PARP	Cell Signaling Technology	Cat# 9548T; RRID: N/A
Cytochrome c	Cell Signaling Technology	Cat# 4272S; RRID: AB_2090454
ATF4	Cell Signaling Technology	Cat# 11815S; RRID: AB_2616025
β-actin	Cell Signaling Technology	Cat# 3700S; RRID: AB_2242334
Anti-Mouse IgG, HRP-linked antibody	Cell Signaling Technology	Cat# 7076S; RRID: AB_330924
Anti-rabbit IgG, HRP-linked antibody	Cell Signaling Technology	Cat# 7074S; RRID: AB_2099233
Chemicals, peptides, and recombinant proteins		
MitoSOX™ Red Mitochondrial Superoxide Indicator	Thermo Fisher Scientific	Cat# M36008
MitoTracker™ Red CMXRos	Thermo Fisher Scientific	Cat# M7512
Azide fluorescein	Sigma-Aldrich	Cat# 910147-10MG
Tris(3-hydroxypropyltriazolylmethyl) amine	Sigma-Aldrich	Cat# 762342-100MG
(+)- Sodium L- ascorbate	Sigma-Aldrich	Cat# A7631-25G
FITC Annexin V	BioLegend	Cat# 640906
Annexin V Binding Buffer	BioLegend	Cat# 422201
Propidium Iodide	Cayman Chemical	Item No. 14289
MitoTEMPO (Hydrate)	Cayman Chemical	Item No. 16621
Bovine serum albumin (BSA)	VWR	Cat# 97061-420
Carbonyl cyanide 3-chlorophenylhydrazone (CCCP)	Cayman Chemical	Item No. 25458
Critical commercial assays		
JC1 reagent	Cayman Chemical	Item No. 10009908
DNeasy Blood and Tissue Kits	Qiagen	Cat# 69504
RNase A	Qiagen	Cat# 19101
Mitochondria Isolation Kit for Cultured Cells	Thermo Fisher Scientific	Cat# 89874
Hoechst	Thermo Fisher Scientific	Cat# H3570
Paraformaldehyde solution 4% in PBS	Santa Cruz Biotechnology	Cat# sc-281692
Fast SYBR™ Green Master Mix	Thermo Fisher Scientific	Cat# 4385610
Experimental models: Cell lines		
MDA-MB-231	ATCC	HTB-26
MDA-MB-468	ATCC	HTB-132
MDA-MB-436	ATCC	HTB-130
HCC1937	ATCC	CRL-2336
4T1	ATCC	CRL-2539
HS578T	ATCC	HTB-126
MCF 10A	ATCC	CRL-10317

(*Continued on next page*)

Continued

REAGENT or RESOURCE	SOURCE	IDENTIFIER
Experimental models: Organisms/strains		
NOD/SCID mice	Jackson Laboratories	RRID:IMSR_JAX:001303
Oligonucleotides		
MT-ND1: forward: 5′-ACTGCGAGCAGTAGCCCAAA-3′	This paper	N/A
MT-ND1: reverse: 5′-AAGGGGGTTCGGTTGGTCTC-3′	This paper	N/A
HK2: forward: 5′-GGACATCATGCGAGGCAGTG-3′	This paper	N/A
HK2: reverse: 5′-GACTGCCTATCCACACGCTG-3′	This paper	N/A
Software and algorithms		
Prism	GraphPad	https://www.graphpad.com/
NIS-Viewer		https://www.microscope.healthcare.nikon.com/products/software/nis-elements/viewer

RESOURCE AVAILABILITY

Lead contact

Further information and requests for resources and reagents should be directed to and will be reasonably fulfilled by the corresponding author, Samuel G. Awuah (awuah@uky.edu).

Materials availability

This study did not generate new unique reagents.

Data and code availability

Data reported in this paper will be shared by the Lead contact upon request. Any additional information required to reanalyze the data reported in this paper is available from the Lead contact upon request.

This paper does not report original code.

EXPERIMENTAL MODELS AND SUBJECT DETAILS

Cell culture

All cell lines used for this study were purchased from the American Type Culture Collection ATCC and grown in a humidified incubator at 37°C with 5% CO_2. MCF10A and HMEC cells were grown in Lonza's Mammary Epithelial Cell Growth Medium (MEGM) supplemented with Lonza's MEGM bullet kit containing, Bovine Pituitary Extract (BPE), human epidermal growth factor (hEGF), insulin, hydrocortisone and Gentamicin-Amphotericin (GA-1000). MDA-MB-468 and MDA-MB-231 cells were maintained in Dulbecco's modified Eagle's medium (DMEM) supplemented with 10% FBS, 1% penicillin/streptomycin and 1% amphotericin. HCC and 4T1 cells were maintained in RPMI supplemented with 10% FBS, 1% penicillin/streptomycin and 1% amphotericin and 4mM glutamine. All the supplements used were purchased from Corning Inc. PBS and trypsin-EDTA used for cell culture maintenance were also purchased from Corning Inc. and used as purchased.

In vivo animal studies

Female, 6 weeks old NOD/SCID mice purchased from Jackson Laboratories, were quarantined for 1 week before use and kept in micro-isolator cages (four mice per cage) in a temperature- and humidity-controlled environment as per the Division of Laboratory Animal Research (DLAR) of University of Kentucky. Under the care of DLAR of University of Kentucky, all mice were maintained in a pathogen-free environment. The study was performed in compliance with the NIH guidelines (NIH Publication No. 85-23 Rev. 1985) for the care

and use of laboratory animals and all experimental procedures were monitored and approved by the Institutional Animal Care and Use Committee (IACUC) of University of Kentucky (USA).

METHOD DETAILS

Chemistry

All solvents used for this study were of ACS grade and used as purchased from Pharmco-Aaper without further purification. All chemicals were purchased from Sigma-Aldrich unless indicated differently. All reactions and experiment were carried out in air under standard atmospheric condition unless indicated differently. Nuclear magnetic resonance (NMR) spectra were obtained at room temperature on Bruker Avance NEO 400 MHz spectrometer. Chemical shift and coupling constant are represented in ppm and Hz respectively. The multiplicity of the signals are represented as singlet (s), doublet (d), m (multiplet) and broad (br). Dichloro (2-benzoylpyridine)gold(III) **1** was synthesized as previously described(Kim et al., 2019). (2-benzoylpyridine)[(2,3-*tert*-butylmethylphosphino)quinoxaline]gold(III)dichloride (AuPHOS-19) was synthesized as previously described with full characterization(Kim et al., 2019). The purity of the synthesized compounds were determined by reversed-phase HPLC (RP-HPLC) (Agilent Technologies 1,100 series HPLC instrument with an Agilent Phase Eclipse Plus C18 column (4.6 mm × 100 mm; 3.5 μm particle size).

*Synthesis of cyclometalated-gold alkyne complex (**3**)*

Dichloro (2-benzoylpyridine) gold(III) (100 mg, 0.22 mmol) and **O-(Prop-2-yn-1-yl) hydroxylamine hydrochloride** (40 mg, 0.421 mmol) was suspended in DCM/MeOH (1:1) total volume of 6mL and stirred at room temperature for 48hrs. The resulting mixture was transferred into a centrifuge tube and centrifuged briefly to separate the precipitate from the filtrate. The filtrate was removed by decanting and the precipitate was washed by resuspending it in equal volume of DCM/MeOH (1:1), centrifuged and the filtrate decanted. The wash step was carefully done 3 times after which the precipitate was finally dissolved in DCM and dried under vacuum (40°C). The product (**2**) is off-white, yield (52mg, 46%). ^{1}H NMR (400 MHz, DMSO-d6) δ 9.34 (d, J = 6.3 Hz, 1H), 8.47 (td, J = 7.8, 1.5 Hz, 1H), 8.32–8.27 (m, 1H), 7.97–7.89 (m, 1H), 7.54 (d, J = 9.0 Hz, 1H), 7.41–7.27 (m, 3H), 5.02 (d, J = 2.4 Hz, 2H), 3.67 (t, J = 2.4 Hz, 1H). ^{13}C NMR (101 MHz, DMSO) δ 153.25, 143.68, 137.88, 133.77, 130.45, 129.16, 128.91, 128.23, 79.59, 79.37, 63.72.

Synthesis of AuPhos-19-AP

To a small scintillation vial was added compound **2** (50mg, 0.11mmol) followed by DCM (10 mL). A white suspension formed which was sonicated for 30 s to dissolve completely. To this mixture was added (R,R)-(−)-2,3-bis (t-butylmethylphosphino) quinoxaline (38.4mg, 0.115) and the reaction was left to stir at room temperature for 10mins after which the reaction was stopped, and the solvent was evaporated on the rotovap to concentrate. This was followed by purification with flash silica gel-chromatography (eluent is 5% MeOH in DCM) to yield product (43 mg, 53.6%).

^{1}H NMR (400 MHz, DMSO-d_6) δ 8.73 (d, *J* = 5.0 Hz, 1H), 8.48 (t, *J* = 8.1 Hz, 2H), 8.33–8.23 (m, 3H), 7.95 (t, *J* = 6.9 Hz, 1H), 7.88–7.73 (m, 2H), 7.56–7.41 (m, 3H), 7.32 (d, *J* = 7.8 Hz, 1H), 7.24 (t, *J* = 7.6 Hz, 1H), 4.72 (d, *J* = 18.1 Hz, 2H), 3.40 (s, 1H), 2.55 (d, *J* = 12.2 Hz, 3H), 2.44 (s, 1H), 1.38 (d, *J* = 17.4 Hz, 12H), 1.27–1.05 (m, 12H. ^{13}C NMR (101 MHz, DMSO) δ 153.09, 150.30, 149.93, 137.31, 135.73, 135.43, 130.50, 127.33, 124.21, 79.95, 79.46, 79.35, 62.68, 40.56, 40.36, 40.15, 39.94, 39.73, 39.52, 39.31, 37.93, 37.70, 37.13, 27.31, 27.28, 27.02, 26.83, 26.78, 8.01, 7.68, 4.79. ^{31}P NMR (162 MHz, DMSO) δ 50.63, 48.19, 46.30, 41.90.

HRMS (ESI) (*m/z*): calcd. for $C_{33}H_{39}AuClN_4OP_2$ [M^+] 801.1953, found: 801.1957. Purity was determined to be >97% by RP-HPLC: R_f = 15.4 min using the following method: Flow rate: 1 mL/min; λ = 260 nm; Eluent A = H_2O with 0.1% TFA; Eluent B = ACN with 0.05% Formic Acid; Solvent Gradient: 0–1 min (97:3H_2O:ACN), 5 min (95:5H_2O:ACN), 8 min (90:10H_2O:ACN), 12 min (80:20H_2O:ACN), 15 min (50:50H_2O:ACN) 17 min (30:70H_2O:ACN) 18mins until end of run (20:80H_2O:ACN).

Cell viability assay

Cell viability was assessed using the MTT (3-(4,5-dimethylthiazol-2-yl)-2,5-diphenyl-2H-tetrazolium bromide) assay. The TNBC and normal cells were seeded in 96-well plates (3,000 cells/well) with DMEM or RPMI and allowed to adhere for 24 h. AuPhos-19 was prepared as a stock (1 mM) in DMSO/media mixture. The compound was added at increasing concentrations with the highest concentration of 30 μM and seven

serial dilutions (1/3x). The cells were placed in the incubator at 37°C with 5% CO_2 for 72 h. After incubation time, the medium was removed and MTT solution was added at a final concentration of 0.5 mg/mL to the wells followed by incubation for 4 h. After incubation, the MTT reagent was carefully removed and 100 μL of DMSO was added to dissolve the formazan crystals. The absorbance was measured at 570 nm using the Biotek plate reader (λ = 570 nm). The experiment was performed in triplicate and the IC_{50} values were calculated using GraphPad Prism software. Mean ± SEM (n = 3).

Apoptosis analysis

MDA-MB-468 and 4T1 cells were seeded at a density of 5 × 10^5 cells/well in 6-well clear bottom plates. The cells were allowed to adhere overnight at 37°C. AuPhos-19 was prepared as a stock (1 mM) in DMSO/media mixture and added to the wells at a concentration of 0.5 μM and incubated for 24 h at 37°C. H_2O_2, used as a positive control was prepared and treated in a separate well at a final concentration of 200 μM. After incubation, the media was collected into separate 15 mL tubes and the wells containing the cells were washed with 2 mL of PBS and transferred into the 15 mL tubes. The cells were detached by trypsinization and added to the tubes also. The tubes were centrifuged for 5 min to form pellets after which the supernatant was removed and the pellets were resuspended in media (5 mL) and counted to make a new solution of 1 × 10^5 cells/mL. The new solution was centrifuged to form pellets. The pellets were resuspended in 300 μL of Annexin binding buffer. To each tube, 5 μL of Annexin V-FITC and 5 μL PI were added and incubated in the dark for 5 min before flow cytometry analysis.

Immunoblotting

The cells were seeded at equal numbers and allowed to adhere and grow to 80% confluence after which the cells were treated with AuPhos-19 1 μM at different for 24 h. After 24 h, cells were washed twice with PBS, then RIPA buffer was added, and cells were scraped and collected into 1.5 mL centrifuge tubes and kept. The mixture was centrifuged for 15 min at 14,000 g and the supernatant was separated from the debris. The cell lysates with equal amount of protein were reconstituted in Laemmli Buffer and heated at 90°C for 10 min. The protein mixture was then separated by 4–20% SDS-polyacrylamide gel electrophoresis (35 min, 100 V) and transferred to PDVF membrane (1 h, 350 mA). The membrane was then blocked with 5% (w/v) bovine serum albumin (BSA) in PBST for 1 h followed by incubation of the membranes overnight with primary antibodies overnight at 4°C. The following day, the membranes were washed three times with PBST and incubated with horseradish peroxidase-conjugated secondary antibodies (r.t, 1 h) prepared in BSA blocking solution. The membranes were washed with PBST (3x for 5 min) after incubation with secondary antibody. The membranes were placed in pierce enhanced chemiluminescence substrate and visualized with Bio-Rad imager. All antibodies used for this study were purchased from cell signaling technology. The primary antibodies are AMPKα (CST, #2532S), ACC (CST, #3662S), mTOR (CST, #2972S), Cleaved PARP, (CST, #9548T), Cytochrome *c* (CST, #4272S), ATF4, (CST, #11815S) and β-actin (CST, #3700S).

Cell cycle

In a 6-well plate, MDA-MB-468 cells were seeded at a density of 2 × 10^5 cells/well and allowed to adhere overnight at 37°C. AuPhos-19 was prepared fresh as a stock in DMSO and added at a final concentration of 0.3 and 0.6 μM. Cells were treated with AuPhos-19 for 12 h. After incubation with AuPhos-19 for 12 h, the medium was removed and added to a 15 mL centrifuge tube. The wells were washed with 2 mL of PBS and added to the centrifuge tube. The cells were detached by adding trypsin (1 mL) and added 4 mL of fresh DMEM. All media were combined, and the tube was centrifuged at 2000 rpm for 5 min to collect the pellet. The media were decanted, and the pellet was suspended in 1 mL of PBS, which was then transferred to a 1 mL Eppendorf tube and centrifuged at 2000 rpm for 5 min to form pellets. The pellets were suspended in 70% EtOH/PBS solution and the solution was stored at 4°C until ready for analysis. After collecting all treatment, the cells were centrifuged at 2000 rpm for 5 min to form pellets. The cells were washed twice with PBS (1 mL) and suspended in 200 μL of a 50 μg/mL PI solution, 50 μL of RNase solution (100 μg/mL) was added. The solutions were then filtered through a 5 mL polystyrene round bottom FACS tube fit with a cell-strainer cap. The samples were analyzed with FACS. Experiment was conducted in triplicates, percentages plotted as the mean ± SD (n = 3).

Whole-cell uptake studies

MDA-MB-468 cells were seeded at a density of 5 × 10^5/well in a 6-well plate and incubated overnight to adhere. The cells were then incubated with the AuPhos-19 (1 μM or 2 μM) in fresh media (RPMI or

DMEM) for 18h at 37°C. The media was removed, and cells were collected via trypsinization. The cells were then washed with PBS (3 × 1 mL) followed by digestion by adding 0.1–0.2 mL of 70% HNO_3. This was briefly sonicated, and the cell solution was diluted to an appropriate concentration using DI water. Analysis of gold content was done by GF-AAS to obtain the whole cell uptake after quantification.

Mitochondrial uptake assay

For mitochondrial uptake, MDA-MB-468 cells (20×10^6) were treated with 1 or 2μM of AuPhos-19 and incubated for 18 h at 37°C. The medium was removed, and the cells were washed with PBS solution (1 mL × 3), trypsinized, and centrifuged. Mitochondria extraction from the cells was then done using the mitochondria extraction kit (ThermoFisher Scientific) according to the manufacturer's protocol. The separated mitochondria pellets were mineralized with 70% HNO_3 followed by dilution with DI water as needed. Analysis of gold content was done by GF-AAS and cellular gold levels were expressed as pmol of Au per million cells.

Colony formation assay

MDA-MB-468 and 4T1 cells were plated in 6 wells plate at 1,000 cells per well. Cells were cultured with and without compound (AuPhos-19) for 10 days. After incubation period cells were fixed with 4% paraformaldehyde for 20 min and stained with crystal violet for 15 min and the number of colonies were counted.

Bioenergetics measurement with seahorse XF96 analysis

TNBC cells were seeded at 30,000 cells/well for the Seahorse XF96 experiments. The cells were seeded a day prior to the experiment in a 100 μL volume per well and incubated overnight at 37°C. AuPhos-19 was prepared as a 1mM stock in DMSO and phenol red free DMEM and diluted to a working concentration with Seahorse XF96 assay buffer. The assay involved a pneumatic injection method of AuPhos-19, with the final injection concentrations of 3 and 6 μM. This was followed by injection of oligomycin (1.5 μM), FCCP (0.6 μM) and rotenone/antimycin A (0.5 μM). The metabolic parameters are calculated based on readings gotten from a minimum of three wells.

Fluorescence visualization of AuPhos-19 compound in cells

Procedure was adapted from previous reports(Hong et al., 2010; Tyler et al., 2017). Cells were seeded at 3×10^5 cells/mL on 35 mm glass-bottom Petri dishes and incubated overnight in appropriate growth medium at 37°C. After adhering overnight, media was removed and cells were washed with PBS twice before treatment with AuPhos-19 at 20 μM for 1 h, the control dish was left untreated. After treatment with test compound, cells were washed three times with PBS followed by treatment with mitotracker red (200 nM) for 45 min after which the cells were washed three times and fixed with 4% PFA for 20 min. After fixing, cells were washed three times and permeabilized with 0.2% triton-X for 1 h at room temperature. Cells were washed three times with PBS after permeabilization.

In a 15 mL centrifuge tube, azide fluorescein (final concentration of 100 μM) and amino guanidine (final concentration of 1 mM) were mixed in PBS, (total reaction volume of 3mL) placed on ice. To this mixture was added $CuSO_4$ and THPTA (molar ratio of 1:5). A stock solution of sodium ascorbate (100 mM) was prepared fresh and added to the mixture for a final ascorbate concentration of (2.5 mM) in the mixture. The reaction mixture was placed on ice for 10 min after which it was added to the cells for 30 min (cells were placed on ice). After 30 min, cells were washed three times and the Hoechst dye was added for 15 min to stain the nuclei. Cells were washed with PBS and mounted on the Nikon A1R confocal microscope with 60X oil objective Images were analyzed with NIS viewer.

Assessment of mitochondria DNA levels

Total DNA was isolated from MDA-MB-468 cells using the DNeasy blood and tissue kit (QIAGEN). The DNA concentration and purity were determined on a Nanodrop Lite (Thermo Fisher Scientific). Real-time PCR was performed to examine the relative amount of mtDNA as described previously(Djeungoue-Petga et al., 2019). Primers sequences for the mitochondrial gene *MT-ND1* were: forward: 5′-ACTGCGAGCAG TAGCCCAAA-3′, reverse: 5′-AAGGGGGTTCGGTTGGTCTC-3′. Primers for the nuclear gene *HK2* were forward: 5′-GGACATCATGCGAGGCAGTG-3′, reverse: 5′-GACTGCCTATCCACACGCTG-3′. The PCR was performed in 10 μL reaction volume containing 2 mM $MgCl_2$, 0.5 μM each of the forward and reverse primers, 4 μL of DNA (5 ng) and 1 μL of master mixture (LightCycler-Fast Start DNA master SYBR Green I; Roche) containing TaqDNA polymerase, deoxynucleotide triphosphates and SYBR Green I. The reaction

was conducted as follows: an initial denaturing step at 95°C for 3 min, followed by 50 cycles at 95 °C for 10 s, 60 °C for 30 s, with acquisition mode at segment 2. Samples were analyzed in triplicate and the number of copies of mtDNA was calculated as $2 \times 2^{\Delta Ct}$, where $\Delta Ct = Ct_{HK2} - Ct_{ND1}$(Quiros et al., 2017).

Mitochondria membrane potential (JC1 assay)

MDA-MB-468, MDA-MB-231 and HMEC cells were seeded at a density of 5×10^5 cells/well in a 6 well plate and allowed to adhere overnight at 37°C. AuPhos-19 was prepared as a stock in DMSO/DMEM and treated at final concentrations of 5 and 10 μM. The cells were incubated at 37°C (5% CO_2) for 1 h. For a positive control, carbonyl cyanide 3-chlorophenylhydrazone (CCCP) was prepared as a stock in DMSO and added at a final concentration of 100 μM for 1 h. After an hour, the cells were trypsinized and resuspended in 2mL PBS. A working solution of the JC-1 dye (Cayman Chemicals, Cat. #15003) was prepared by adding 100 μL of dye into 900 μL of DMEM. The cells were then exposed to 100 μL/mL of working solution of the JC-1 dye (avoid direct exposure to light) and incubated at 37°C for 15 min. This was followed by analysis on a flow cytometer with 488 nm excitation and appropriate emission filters.

Mitochondria ROS (mtROS)

MDA-MB231 and MDA-MB 468 cells were plated in six wells plate at 500,000 cells per well and allowed to adhere overnight. Cells were treated with AuPhos −19 for short period of 2 h at concentrations of 2 μM. In one well, cells were treated with mitotempo (2 μM) for 1h, media was removed before treatment with compound. After incubation time with test compound, cells were trypsinized and centrifuged to form pellets. Pellets were washed with PBS and resuspended in Mitosox dye solution (200 μL). This was transferred into FACS tube and incubated for 20mins followed by flow cytometry analysis.

In vivo experiment of AuPhos-19

Female, 6-week-old NOD/SCID mice were purchased from Jackson Laboratories, and they had an acclimation period of one week before inoculation with 1,000,000 4T1-iRFP cells subcutaneously on their flanks. Three days post-implantation, the mice were systemically treated with 10 mg/kg AuPhos-19 via intraperitoneal administration, 0.1 mL/mouse formulated as DMSO (1%), Kolliphor (10%), and PBS (89%). The control group was treated with a PBS solution containing 1% DMSO and 10% Kolliphor. The injection of AuPhos-19 was performed three times a week for two weeks. Tumor volume was measured and calculated according to the following formula:

$〚V0(mm)〛 \wedge 3) = ([〚Width(mm)〛 \wedge 2 \times Length(mm)])/2$ by external calipers. Body-weight of mice under the treatment duration was performed every other day, and mice were euthanized 19 days later. (n = 4 for AuPhos-19-treated, and n = 4 for vehicle control).

QUANTIFICATION AND STATISTICAL ANALYSIS

Statistical analysis, methods and details for each experiment are in the legend of each figure. Analysis was done using GraphPad Prism 9.0 by two-tailed unpaired Student's *t* test, ordinary one-way ANOVA or two-way ANOVA followed by Dunnett's multiple comparison test.